Structural and defect characterization of CuInS$_2$ single crystals grown under elevated pressures*

N. Dietz, M. L. Fearheiley, S. Schroetter and H. J. Lewerenz

Hahn-Meitner-Institut, Bereich Photochemische Energieumwandlung, Glienicker Strasse 100, 1000 Berlin 39 (Germany)

(Received January 21, 1992)

Abstract

By using an argon overpressure, large CuInS$_2$ single crystals were produced. Upon modification of the temperature gradient over the melt a change of structural features was induced. Low temperature gradients resulted in the growth of large single crystals, whereas for increased temperature gradients sheet-like material was prepared. The lamellar material cleaved along the (112) planes as revealed by reflection high-energy electron diffraction, and the appearance of Kikuchi lines indicates good crystallinity. Within the limits of X-ray diffraction the material was shown to be single-phase CuInS$_2$. IR measurements were employed for comparison of materials with different structural properties. Possible origins for the new lamellar structure are discussed. Additional information obtained by a new angle-resolved reflection spectroscopy on the defects in CuInS$_2$ single crystals is presented. The method permits the room temperature detection of small variations of the complex dielectric function ε. The variation of $\varepsilon = \varepsilon_1 + i\varepsilon_2$ is correlated to the defect centres and their energetic position in the band gap. The defect levels determined from this method are compared with photoluminescence and transmission spectroscopy results.

1. Introduction

CuInS$_2$ has received attention as a possible alternative base material for solar cells [1–8]. At room temperature CuInS$_2$ has the chalcopyrite structure and possesses a band gap of 1.55 eV, which lies near the optimum for homojunction solar cell devices [9]. The first highly photoactive material in a non-optimum configuration has been reported from our laboratory [8]. Recently a thin film device has been produced exhibiting a 7.3% power conversion efficiency [10].

For applications in high-efficiency energy-converting systems, such as concentrators, the growth of high quality single-crystalline material is mandatory. With a direct energy gap in the optimum range of the theoretical solar conversion efficiency ($E_g = 1.55$ eV) a minority carrier diffusion length of about 2 μm would be sufficient for effective carrier collection in the relevant spectral range [11, 12].

The performance of CuInS$_2$ solar cells has lagged behind that of its selenide analogue, whose solar-to-electrical conversion efficiency has reached 14% [13].

Among the differences in material preparation of the sulphur and selenide chalcopyrite is the significant variation of the chalcogenide vapour pressure. Owing to the higher vapour pressure of sulphur, similar growth conditions as for CuInSe$_2$ can only be expected for growth in inert atmosphere at elevated pressure as this reduces the sulphur partial pressure.

The analysis of electronic defects is of crucial importance for semiconductor material development. To satisfy the requirement of defect characterization in electronic devices and their components, a series of optical detection methods was developed. These methods, for example photoluminescence [14–20], electroreflectance [21, 22], photoreflectance [14, 23], standard reflectivity [14, 24] and absorption measurements [25], are limited in sensitivity or applicability. To develop new materials for solar applications, different methods are necessary to tailor its production conditions. Therefore we have developed an experimental method based on the measurement of the Brewster angle (also called pseudo-Brewster angle [26] or first Brewster angle [27]) ϕ_B and the reflectivity R_p for light polarized parallel to the plane of incidence. The method allows accurate determination of the optical constants ε_1 and ε_2 as well as small variations in the optical constants, which result from defects whose energy levels lie within the band gap.

2. Material preparation

The gradient freeze technique [28] was used to grow CuInS₂ single crystals. A thick-walled quartz ampoule containing the reactants was evacuated and refilled twice with argon, and the third argon fill was condensed using liquid nitrogen. The resulting argon pressure in the ampoule was calculated to be around 5 bar at room temperature. A two-zone oven was used for the growth experiments in order to control independently the temperature of the metals and sulphur. The Cu–In zone was heated to a temperature of 800 °C; then the sulphur zone was heated to 450 °C at a rate of between 50 and 100 °C h^{-1}. After the constituents had reacted, the temperature of both zones was raised to 1100 °C at a rate of 50 °C h^{-1}. At this temperature the argon pressure is approximately 25 bar. The melt was allowed to homogenize for approximately 21 h, then cooled at a rate from 1 to 5 °C h^{-1} through the melting point (1090 °C), and then quickly cooled to the next transition point (1045 °C), where the rate was once again reduced to 1–5 °C h^{-1}. This was repeated a third time at 980 °C; then the sample was cooled to room temperature.

The amount of the starting material remained the same as the position of the boat was varied in the temperature gradient. This gradient ranged from 2 to 15 °C cm^{-1} and experiments without an argon overpressure were also carried out. The growth runs resulted in two different surface morphologies.

3. Structural analysis

By using an argon overpressure (25 bar at the melting point) during the growth of CuInS₂ from its melt, we were able to grow large single crystals. This process led to two types of crystal depending on the temperature gradient above the liquid–melt interface. For moderate temperature gradients, single crystals on the order of 10×10×3 mm^3 were obtained. For steeper temperature gradients, crystals possessing a lamellar-type structure were obtained (Fig. 1). Surprisingly, both types of sample could be easily cleaved, which is not expected for a chalcopyrite structure. The comparison of Debye–Scherrer diffraction data with file data shows both materials to be single-phase CuInS₂ within the experimental limitations of the method. The lattice constants inferred from the data are $a = 5.760$ Å and $c = 11.50$ Å. Laue diffraction patterns obtained from a cleaved sample show [112] orientation, an indication that cleavage occurs predominantly along (112) planes. The natural cleavage planes for CuInS₂ are (110) orientated [29, 30]. The quality of the crystals can be seen most readily from X-ray and electron microscopic
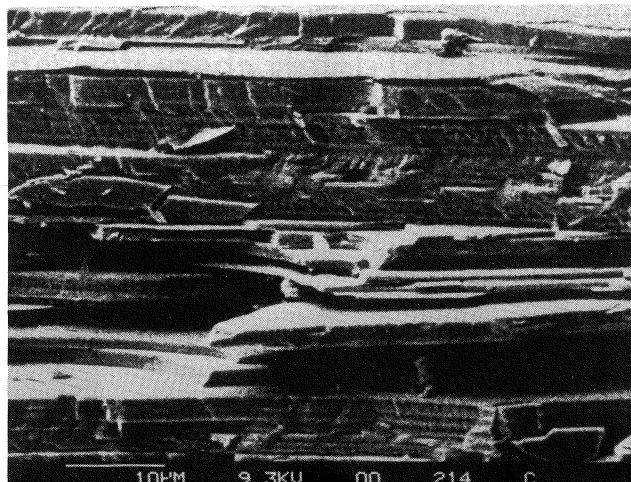
Fig. 1. Scanning electron micrograph of the lamellar-type material.
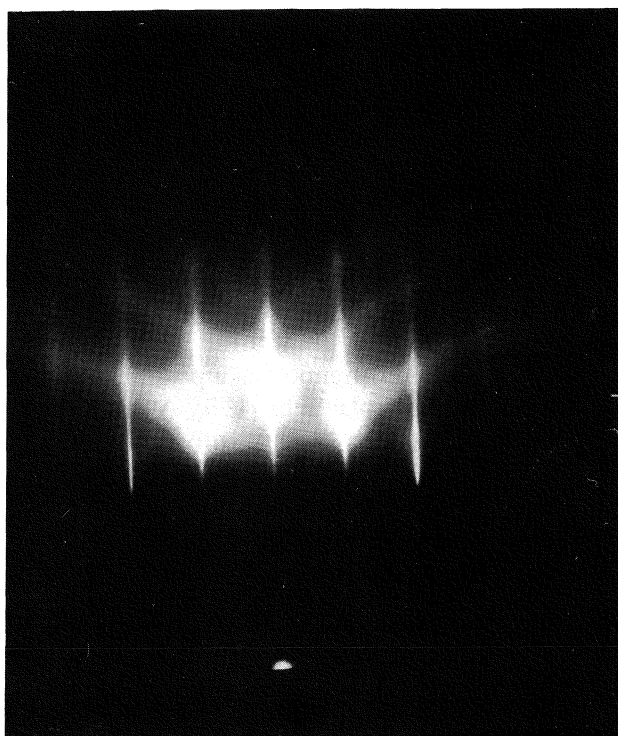
Fig. 2. RHEED pattern arising from the (112) planes of CuInS₂ lamellar-type material.

analyses. The observance of Kikuchi lines (Fig. 2) requires a high perfection of the crystals; otherwise defects would spread these lines over larger angles. The data confirm the [112] orientation of the cleavage planes. The occurrence of Kikuchi lines demonstrates quite high crystallinity over extended regions of the sample. The lattice constant determined from the reflection high-energy electron diffraction (RHEED) experiment is $a = 5.76$ Å with $c/a = 2.04$.

Rocking curves were produced to determine the relative dislocation density. A full width at half-maximum of $1140''$ is indicative of a structure containing substantial amounts of dislocations, possibly also microcrystallites. The influence of the modification of growth parameters on the structural characteristic has also been investigated. The apparent contradiction between our RHEED and rocking curve results can be resolved with the following argument. RHEED is a surface technique; electrons impinging at low angles on the surface interact with only surface and near-surface atoms. Thus the surface shows good crystallinity. Rocking curves, on the other hand, indicate a high density of dislocations. However, these experiments expose the whole sample to the X-rays. Therefore these results reflect the condition of the bulk of the sample and indicate the existence of a high degree of dislocation.

Although X-ray diffraction and electron microprobe analysis showed the material to be CuInS₂, within their respective limits, the material exhibited a mechanical behaviour different from the expected behaviour for CuInS₂. The cleavage of the material yielded very thin layers which could be peeled off with adhesive tape, similar to the procedures known for layered crystals such as WSe₂. An analysis of the (112) planes after cleavage *in vacuo* by X-ray photoelectron spectroscopy revealed large deviations of the copper-to-indium ratio from unity [31]. The electron penetration depth is of the order of ten atomic layers and the fact that the copper-to-indium ratio is not consistent on both cleaved surfaces means the interphase is probably only a few atomic layers thick, less than the escape depth of photoelectrons. This phase could have formed during freezing as a result of the stressed environment brought about by the steep temperature gradient and/or high pressures. The nature of this phase is currently under investigation.

Twin formation is a function of thermal, constitutional and orientational conditions during solidification from the melt. Thermal stresses which develop during growth promote the formation of twins, and when these stresses are combined with constitutional supercooling the development of twin lamellae is observed. The occurrence of twin lamellae during growth of germanium has previously been observed [32]. For CuInS₂, the preferred growth direction is the $\langle 100 \rangle$, whereas growth in the $\langle 112 \rangle$ direction is relatively slow. Under the condition of constitutional supercooling, to maintain the interface at the freezing point isotherm the growth is easiest parallel to the {112} planes. These twin lamellae grow inwards to absorb the supercooling and in the $\langle 112 \rangle$ direction, where growth is slow, twins are formed in order to adjust to the freezing point isotherm. The conditions responsible for these twin lamellae are currently under investigation.

4. IR measurements

4.1. Experimental details

The IR spectra were obtained with a Bruker 113v Fourier transform spectrometer equipped with an SiC globar source for the middle IR (MIR) (between 5000 and 500 cm⁻¹), and a mercury lamp as source for the far IR (FIR) (between 500 and 50 cm⁻¹) respectively. Different deuterium triglycerinsulfide (DTGS) detectors were used for the two spectral regions. The spectra were taken with a resolution of $\Delta \nu = 4$ cm⁻¹ and consist of 256 (MIR) or 512 (FIR) scans. The measurements were performed in both transmission and reflection mode; in reflection a standard sample holder for variable angles was used with an aluminium-coated mirror as reference and a KRS-5 polarizer.

4.2. Discussion of results

In the MIR, for all samples the well-known interference fringes occurred as a result of multiple reflections between the layers (Fig. 3). As described by Harrick [33] these interferences can be used to determine the thickness of the transmitted layers. Assuming a refractive index of 2.51 for CuInS₂ we calculated that the spectrum of Fig. 3 was taken from a sample with $d = 137$ μm. In the FIR, layers of thickness 100–200 μm are absorbing the whole radiation while thinner films with $d \approx 10$ μm are transparent (Fig. 4). In reflection the penetration depth of the IR light is estimated to be between 15 μm (MIR) and 55 μm (FIR) respectively.

Of the 21 optical vibrational modes for CuInS₂, nine modes are IR active [34–36]. Since the chalcopyrite lattice is optically anisotropic for the reflection measurements, it is necessary to consider the orientation of the sample, the angle of incidence and the polarization of the light. For the electrical vector **E** being perpendicular to the **c** axis, two of three expected modes have been reported [34–36]. The **E**∥**c** configuration cannot be realized exactly for crystals cleaved along the (112) plane; therefore Koschel *et al.* [35] extrapolated the spectrum for this orientation yielding three of six expected IR modes. The spectra of Neumann *et al.* [36] coincide with those of Koschel *et al.* [35] although the orientation of the samples (*i.e.* cleavage plane) is not mentioned in the former. For clarity in our experiments we did not make any mathematical extrapolations and therefore our spectra for the normal crystals show the same spectral features as published by Bodnar *et al.* [34]. In the spectra of the lamellar-type material (Figs. 4 and 5) the absorption bands are almost masked by strong interferences but nevertheless an additional mode at 217 cm⁻¹ is observed. IR spectra are available for InS [37], β-In₂S₃ [38], In₆S₇ [39], CuIn₅S₈ [40] and Cu₃In₅S₉ [41] but for none of them was an absorption at 217 cm⁻¹ reported.
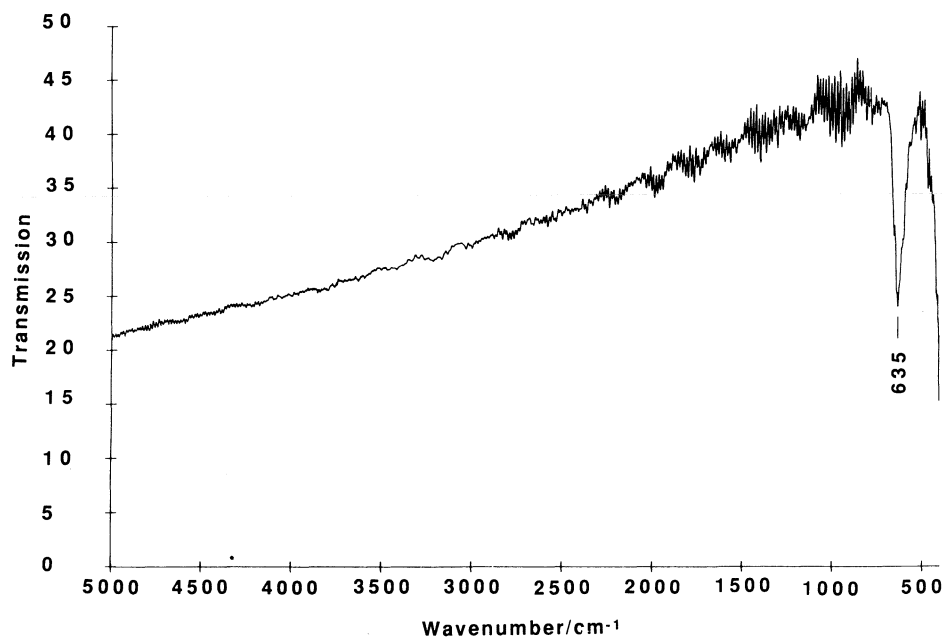
Fig. 3. Transmission IR spectrum of a lamellar-type CuInS$_2$ layer with $d = 137\ \mu$m (MIR).
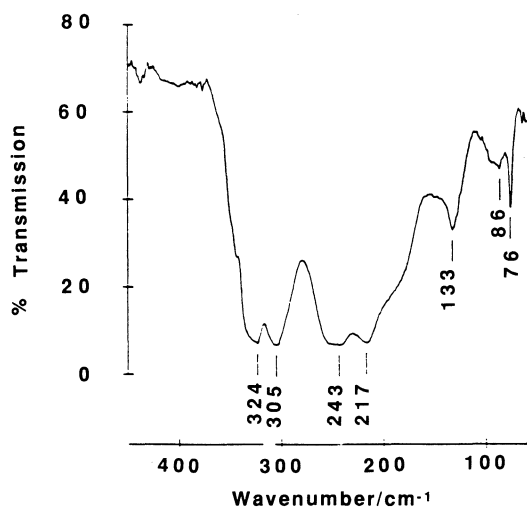
Fig. 4. Transmission IR spectrum of a lamellar-type CuInS$_2$ layer of about 10 μm thickness (FIR).

5. Brewster angle spectroscopy (BAS) and photoluminescence

5.1. Experimental details

The optical constants were obtained by BAS [42, 43] in an energy range from 0.7 to 1.8 eV. The schematic diagram of the experimental set-up is shown in Fig. 6. A W–I lamp was used as light source in combination with a Kratos monochromator. The monochromatic beam is split into a reference and a signal beam. The signal beam is polarized parallel to the plane of incidence using a Glan–Thompson polarizer P. The polarized light is focused onto a mirror-type
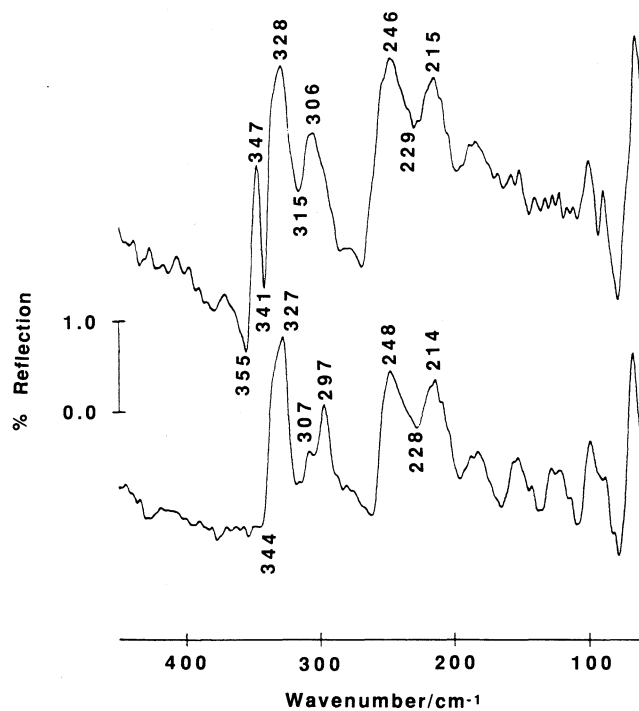
Fig. 5. IR reflectivity spectra of CuInS$_2$ (lamellar-type material): upper curve, approximately $\mathbf{E} \perp \mathbf{c}$; lower curve, approximately $\mathbf{E} \parallel \mathbf{c}$.

specularly reflecting sample which is held at an angle ϕ close to the Brewster angle ϕ_B. The reflected intensity is detected by a cooled silicon (0.4–1 μm) or germanium (0.8–1.7 μm) detector. For analysis of the reflected intensity and the Brewster angle position, the signal beam was measured as a function of the angle ϕ.
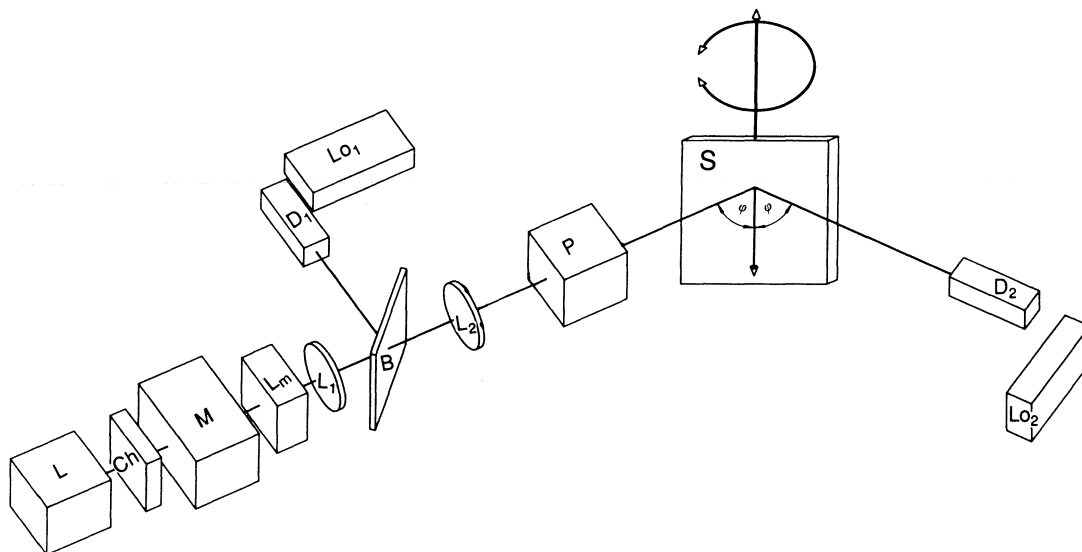
Fig. 6. Schematic diagram of the experimental set-up: L, lamp; Ch, chopper; M, monochromator; L_m, achromatic lens system; L_1, L_2, slits; B, beam splitter; P, polarizer; D_1, D_2; detectors; L_{0_1}, L_{0_2}; preamplifier; S, sample.

The minimum was determined by a least-squares fit and the reflectivity R_p was determined by comparison with the reference beam. A standard lock-in technique was used for data acquisition.

Comparative photoluminescence measurements were performed by using an excimer laser (EMG 53 MSC, Lamda Physics) to pump a dye laser (FL 2001, Lamda Physics). The excitation energy was 2.3 eV, the beam power 18 mW. The samples were mounted into a TIC 303M (Cryovac) continuous-flow liquid helium cryostat. The emission spectra were recorded using a Spex 1401 monochromator and photomultiplier (RCA 7071).

Supplementary transmission measurements were made with an Omega spectral photometer (Bruin Instruments) using the two-beam reference method in an energy range from 0.70 to 4 eV.

5.2. Results of optical defect characterization

5.2.1. GaAs

To test the sensitivity as well as the accuracy of the BAS method, the defect structures of GaAs, which have already been reported [44–47], were investigated. Figure 7(a) shows the spectral dependence of the Brewster angle ϕ_B and the reflectivity R_p at ϕ_B for n-GaAs (100) with a carrier concentration smaller than 10^{16} cm^{-1}. Below the band gap at $E_g = 1.42$ eV the well-known intrinsic electron traps at 0.78 eV (L_{12}) and 0.83 eV (L_2) and the reported absorption centres at 0.95, 1.10 and 1.30 eV [46] are clearly revealed.

The calculated refractive index n (Fig. 7(b)) compared with data obtained by the prism-diffraction
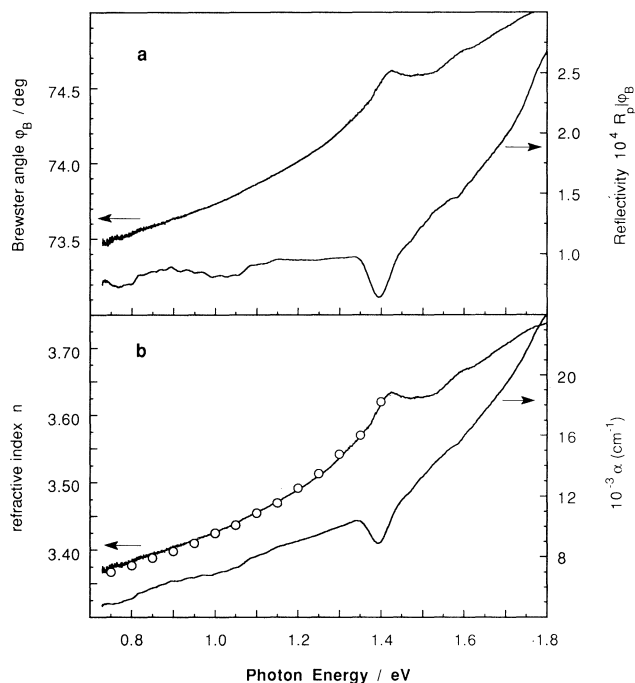
Fig. 7. (a) Measured spectral dependence of the Brewster angle ϕ_B and the reflectivity R_p at ϕ_B for undoped GaAs(100). (b) Refractive index n (compared with literature values [48] (○)) and absorption coefficient α, calculated using the analytical BAS method.

method [48] (open circles) show excellent agreement with an error of less than ± 0.1%. Near the band gap, the absorption coefficient α agrees well with literature values [49, 50]. Below the band gap lower values for the absorption coefficient are reported [51–53].

5.2.2. CuInS₂

Three types of $CuInS_2$ sample were investigated. All samples were grown with the gradient freeze technique [28] using argon overpressure. By variation of the growth conditions [54], crystals which varied from semi-insulating (type A), moderately p-type (type B) to lamellarly structured material were produced. The experimental results for the lamellar structure material will be published elsewhere [55].

For the ternary chalcopyrite $CuInS_2$, the optical properties near the band gap $(E_g = 1.55$ eV) have been studied using measurements of absorption [14, 25, 56], reflectivity [14] electroreflectance and photoreflectance [14, 23]. The defect structures were mostly investigated by photoluminescence measurements [15–17, 20, 57]. The optical defect characterization as a supplement to the usually complex electronic characterization has not yet been performed. To do this, BAS provides a simple and fast method. The sensitivity of this method is shown in Fig. 8 on a reflectivity plot at various angles of incidence ϕ for $CuInS_2$ (type A). For an incidence angle $\phi = 30°$ a broad reflection structure below the band gap at 1.30 eV occurs. With angles closer to the Brewster angle ϕ_B ($\phi = 50°$, $\phi = 60°$ and $\phi = 65°$) several structures can be observed. With an angle $\phi = 70°$ close to the Brewster angle $(\phi_B \approx 69°-71°)$, structure arising from defects is clearly visible. The reflectivity decreases from about 20% at $\phi = 30°$ to values smaller than 1% at $\phi = 70°$. At the Brewster angle, a reflectivity smaller than 10^{-4} is detected. This sequence shows the main advantage of the method.

The spectral dependence of the Brewster angle and the reflectivity at room temperature are shown in Fig. 9(a) for intrinsic as-grown $CuInS_2$ (type A) in the energy range 0.7–1.8 eV. Figure 9(b) shows the calculated refractive index n and the absorption coefficient α. The insert in Fig. 9(b) displays the calculated reflectivity at normal incidence. A direct band gap transition at 1.556 eV was found. Below the band gap well-pronounced deep level centres at 1.32, 1.26, 1.20, 1.15 1.11, 1.06, 1.01, 0.97, 0.92, 0.88 and 0.80 eV were revealed. Using first and second derivatives of the Brewster angle spectra to determine the energy position of the defect centres [58], defect centres at 1.44, 1.38 and 1.32 eV were found.

The variations of the Brewster angle and reflectivity for a p-$CuInS_2$ sample (type B), which is highly self-compensated, are shown in Fig. 10(a). The energetic

Fig. 8. The measured reflectivity R_p for various angles of incidence ($\phi = 30°$, $\phi = 50°$, $\phi = 60°$, $\phi = 70°$) shows the advantages of the method. The reflectivity close to the Brewster angle ϕ_B ($\phi = 70°$) clearly shows absorption centres.
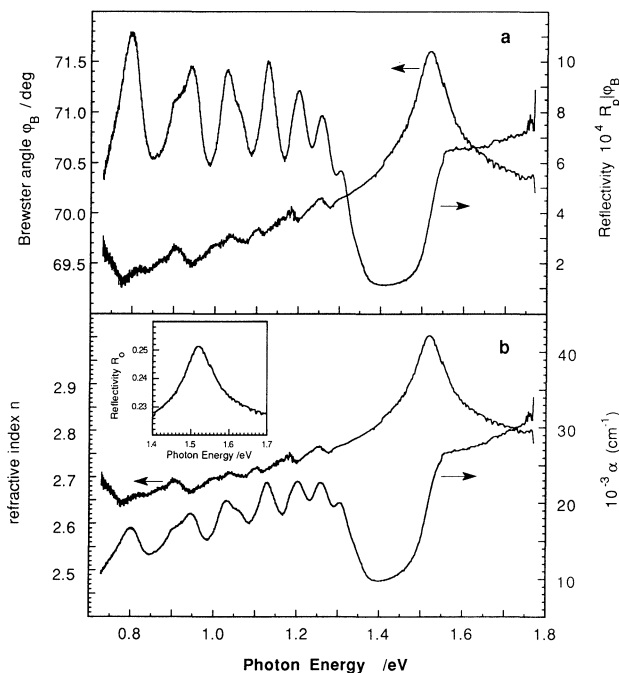
Fig. 9. (a) The measured spectral dependence of the Brewster angle ϕ_B and the reflectivity R_p at ϕ_B for intrinsic as-grown $CuInS_2$ (type A). (b) Calculated refractive index n and the absorption coefficient α. The inset shows the calculated reflectivity at normal incidence R_0 with high accuracy for the band gap region.
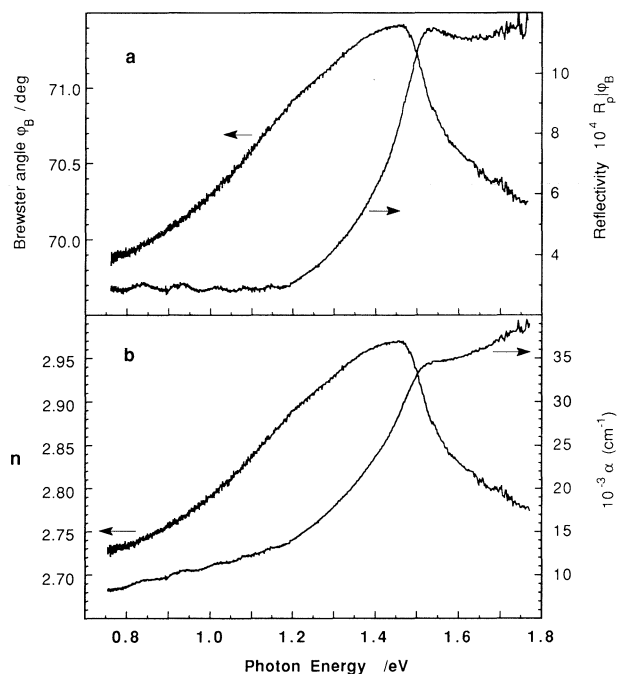
Fig. 10. (a) The spectral dependence of the Brewster angle ϕ_B and the reflectivity R_p at ϕ_B for CuInS$_2$ (type B). (b) Calculated refractive index n and the absorption coefficient α. Here a broad structure below the band gap (at. 1.52 eV) in the refractive index n indicates a high concentration of dislocations.

position of the band gap decreases to 1.52 eV with a flatter band tail than shown in Fig. 9(b). The broad structure in the refractive index n below the band gap indicates a high concentration of dislocations. These dislocations result in a higher absorption in the energy range from 1.2 to 1.6 eV resulting from defect levels centred at 1.44 and 1.38 eV. Below the band tail, absorption centres at 1.146, 1.088, 1.03, 0.94 and 0.84 eV were observed.

The transmission spectra of both types of CuInS$_2$ are shown in Fig. 11. Only a broad absorption structure at about 1.40 eV is detectable. The transmissions below 1.4 eV are associated with the different sample thicknesses. The results are not helpful in identifying the defect levels in the CuInS$_2$ material.

In Fig. 12 the photoluminescence spectra of the two different types of CuInS$_2$ material are shown. The intrinsic single-crystal CuInS$_2$ (type A) in Fig 12(a) shows two emission peaks at 1.435 and 1.40 eV, which lie about 20 meV lower than those earlier reported for indium-rich CuInS$_2$ [16, 17]. The sample also shows a broad emission at about 1.27 eV, which is associated with sulphur excess [59]. The photoluminescence spectra of CuInS$_2$ (type B) in Fig. 12(b) show only one broad emission structure at 1.39 eV, which is correlated to copper excess [16].

These transitions shown in the photoluminescence spectra (Figs. 12(a) and 12(b) do not represent the only
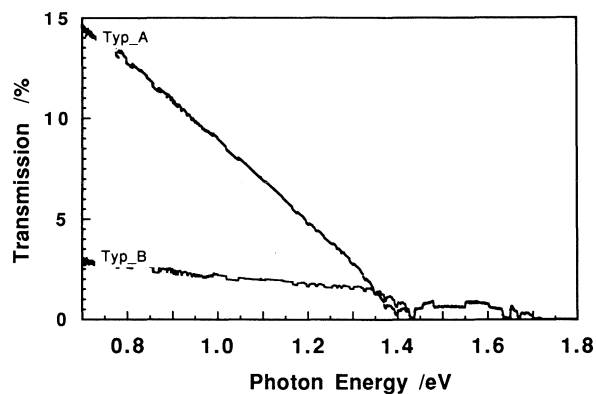
Fig. 11. Transmission spectra for CuInS$_2$ (type A, type B) at room temperature.
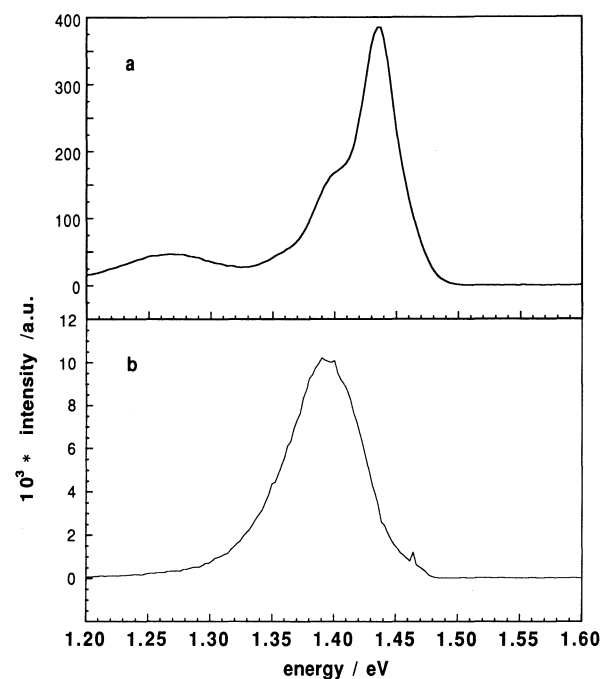
Fig. 12. Photoluminescence spectra at 5 K for (a) type A and (b) type B CuInS$_2$ crystals.

levels present, nor do these emissions indicate the defect concentration of the levels involved. In contrast, the BAS method, through proper modelling [60], reveals much more detail concerning sub-band-gap levels and relative concentrations. Since the changes in the optical properties due to native defects vary independently with the particular defect and its concentration, this method is not as restrictive as standard photoluminescence spectroscopy.

6. Conclusions

It has been shown that large CuInS$_2$ single crystals can be grown using an argon overpressure. Two types

of crystal morphology result, one being normal single crystals and the other a lamellar-type structure. Both structures cleave along the (112) plane. With regard to optical properties, the lamellar-type material exhibits an unaccountable mode at 217 cm^{-1} in the IR, and multiple reflections arising from the layers reveal a 10 μm layer thickness.

It has also been shown that the BAS method provides a powerful tool in investigating deep levels as well as the optical constants of semiconductors. The deep defect levels found by the BAS method provide additional and somewhat complementary information to the emission centres observed by photoluminescence. Both methods, photoluminescence and BAS, are complementary in that the former relies on radiative recombination whereas the latter observes light-induced transitions from and to defects.

Acknowledgments

References

1 L. L. Kazmerski and S. Wagner, Cu–ternary chalcopyrite solar cells, in T. J. Coutts and J. D. Meakin (eds.), *Current Topics in Photovoltaics*, Academic Press, London, 1989, pp. 41–109.

2 C. D. Lokhande and G. Hodes, *Sol. Cells, 21* (1987) 215.

3 D. Cahen, Y. Mirovsky and R. Tenne, *Solid State Chemistry, 1982, Proc. 2nd Euro. Conf., Veldhoven, Netherlands, June 7–9, 1982, Studies in Inorganic Chemistry*, Vol. 3, Elsevier, Amsterdam, 1983.

4 M. Robbins, K. J. Bachmann, V. G. Lambrecht, F. A. Thiel, J. Thomson, R. G. Vadimsky, S. Menezes, A. Heller and B. Miller, *J. Electrochem. Soc., 125* (1978) 832.

5 L. L. Kazmerski and G. A. Sanborn, *J. Appl. Phys., 48* (7) (1977) 3178.

6 A. N. Tiwari, D. K. Pandya and K. L. Chopra, *Sol. Cells, 22* (1987) 263.

7 P. R. Ram, R. Thanggaraj, A. K. Sharma and O. P. Agnihotri, *Sol. Cells, 14* (1985) 123.

8 H. J. Lewerenz, H. Goslowsky, K.-D. Husemann and S. Fiechter, *Nature, 321* (6071) (1986) 687.

9 J. J. Loferski, *J. Appl. Phys., 27* (1956) 777.

10 K. W. Mitchell, G. A. Pollock and A. V. Mason, *Proc. 20th IEEE Photovoltaic Specialists' Conf., Las Vegas, NV*, IEEE, New York, NY, 1988, p. 1542.

11 S. Mora, N. Romeo and L. Tarricone, *Solid State Commun., 29* (1979) 155.

12 R. Scheer, M. Wilhelm and H. J. Lewerenz, *J. Appl. Phys., 66* (11) (1989) 5412.

13 K. Mitchell, C. Eberspacher, J. Ermer and D. Pier, *Proc. 20th IEEE Photovoltaic Specialists' Conf., Las Vegas, NV*, IEEE, New York, NY, 1988, p. 1384.

14 B. Tell, J. L. Shay and H. M. Kasper, *Phys. Rev. B, 4* (8) (1971) 2463.

15 G. Massé, N. Lahlou and C. Butti, *J. Phys. Chem. Solids, 42* (6) (1981) 449–454.

16 J. J. M. Binsma, L. J. Giling and J. Bloem, *J. Lumin., 27* (1982) 35–53.

17 J. J. M. Binsma, L. J. Giling and J. Bloem, *J. Lumin., 27* (1982) 55–72.

18 P. Lange, H. Neff, M. L. Fearheiley and K. J. Bachmann, *J. Electron. Mater., 14* (6) (1985) 667–676.

19 H. J. Hsu, M. H. Yang, R. S. Tang, T. M. Hsu and H. L. Hwang, *J Cryst. Growth, 70* (1984) 427–432.

20 B. Abid, J. R. Gong, H. G. Goslowsky and K. J. Bachmann, *Proc. IEEE Photovoltaic Specialists' Conf.*, 1987, IEEE, New York, NY, p. 1305.

21 T. M. Hsu, S. F. Fan and H. L. Hwang, *Phys. Lett. A, 99* (5) (1983) 255.

22 H. Neff, P. Lange, M. L. Fearheiley and K. J. Bachmann, *Appl. Phys. Lett., 47* (10) (1985) 1089–1091.

23 T. M. Hsu, J. S. Lee and H. L. Hwang, *J. Appl. Phys., 68* (1) (1990) 283–287.

24 B. Tell, J. L. Shay and H. M. Kasper, *J. Appl. Phys., 43* (1972) 2469.

25 L. Y. Sun, L. L. Kazmerski, A. H. Clark, P. J. Ireland and D. W. Morton, *J. Vac. Sci. Technol., 15* (2) (1978) 265–268.

26 R. M. A. Azzam and N. M. Bashara, *Ellipsometry and Polarized Light*, North-Holland, Amsterdam, 1987.

27 H. B. Holl, *J. Opt. Soc. Am., 57* (5) (1967) 683.

28 M. L. Fearheiley and K. J. Bachmann, *Proc. Symp. on Materials and New Processing Technologies for Photovoltaics, San Francisco, CA*, The Electrochemical Soc., Pennington, NJ, 1983, pp. 469–477.

29 M. Sander, H. J. Lewerenz, W. Jeagermann and D. Schmeißer, *Fresenius' Z. Anal. Chem., 329* (1987) 367–369.

30 M. Sander, W. Jaegermann and H. J. Lewerenz, *J. Phys. Chem., 92* (2) (1992) 782–790.

31 N. Dietz and W. Jaegermann, unpublished results, 1990.

32 G. F. Bolling, W. A. Tiller and J. W. Rutter, *Can. J. Phys., 34* (1956) 234–240.

33 N. J. Harrick, *Appl. Opt., 10* (1971) 2344.

34 I. V. Bodnar, A. G. Karoza and G. F. Smirnova, *Phys. Status Solidi B, 86* (1978) K171.

35 W. H. Koschel, F. Sorger and J. Baars, *J. Phys. C, 3* (1975) 177.

36 H. Neumann, W. Kissinger, H. Sobotta, V. Riede, R. D. Tomlinson and N. Avgerinos, *Czech. J. Phys. B, 34* (1984) 69.

37 K. Takarabe, K. Wakamura and T. Ogawa, *J. Phys. Soc. Jpn., 52* (1983) 686.

38 H. D. Lutz and H. Haeuseler, *Z. Naturforsch., Teil A, 26* (1971) 323.

39 N. M. Gasanly, B. M. Dzhavadov, A. S. Ragimov, T. I. Tagirov and R. E. Guseinov, *Phys. Status Solidi B, 106* (1981) K47.

40 N. M. Gasanly, S. A. El-Hakim, L. G. Gasanova and A. Z. Magomedov, *Phys. Status Solidi B, 158* (1990) K1.

41 E. A. Vinogradov, N. M. Gasanly, L. G. Gasanova, A. Z. Magomedov and V. I. Tagirov, *Phys. Status Solidi B, 144* (1987) K73.

42 H. J. Lewerenz and N. Dietz, *Appl. Phys. Lett., 59* (12) (1991) 1470–1472.

43 N. Dietz and H. J. Lewerenz, *Appl. Phys. Lett., 11* (1992) in the press.

44 J. C. Bourgoin and H. J. von Bardeleben, *J. Appl. Phys., 64* (1988) R65-R91.

45 R. Haak and D. Tench, *J. Electrochem. Soc., 131* (1984) 275-283.

46 M. O. Manasreh, W. C. Mitchel and D. W. Fischer, *Appl. Phys. Lett., 55* (1989) 864.

47 N.-I. Nishizawa, Y. Oyama and K. Dezaki, *J. Appl. Phys., 67* (1990) 1884-1896.

48 D. T. F. Marple, *J. Appl. Phys., 35* (1964) 1241.

49 D. E. Aspnes and A. A. Studna, *Phys. Rev. B, 27* (1983) 985-1009.

50 A. Sadao, *J. Appl. Phys., 66* (1989) 6030-6040.

51 D. D. Sell and H. C. Casey, *J. Appl. Phys., 45* (1974) 800.

52 M. D. Sturge, *Phys. Rev., 127* (1962) 768.

53 H. C. Casey, D. D. Sell and K. W. Wecht, *J. Appl. Phys., 46* (1975) 250.

54 M. L. Fearheiley, N. Dietz and H. J. Lewerenz, *J. Electrochem. Soc., 139* (2) (1992) 512.

55 H. J. Lewerenz and N. Dietz, *J. Appl. Phys.*, submitted for publication.

56 A. W. Verheijen, L. J. Giling and J. Bloem, *Mater. Res. Bull., 14* (1979) 237.

57 P. Lange, H. Neff, M. L. Fearheiley and K. J. Bachmann, *Phys. Rev. B, 31* (6) (1985) 4074-4076.

58 N. Dietz, *Ph.D. Thesis*, Technische Universität-Berlin, 1991.

59 H. Goslowsky, S. Fiechter, R. Könenkamp) and H. J. Lewerenz, *Sol. Energy Mater., 13* (1986) 221.

60 N. Dietz and H. J. Lewerenz, submitted to *J. Appl. Phys.*